

## Chapter

# Mineralogy and Geochemistry of Shales of Mamu Formation in Nigeria: Effects of Deposition, Source Rock, and Tectonic Background

*Segun A. Akinyemi, Olajide F. Adebayo, Henry Y. Madukwe, Adeyinka O. Aturamu and Olusola A. OlaOlorun*

## Abstract

Study of lithofacies identification, geochemical characterization of shales is vital to the provenance, paleoweathering, and tectonic setting reconstruction. The combination of morphological analysis, bulk chemical analysis and in-situ multi-element analysis was used to investigate the provenance, source area weathering, and depositional setting of outcropped Maastrichtian shale sequence of the Mamu Formation, Anambra Basin in Nigeria. Ten representative shale samples were examined by scanning electron microscopy/energy dispersive spectroscopy (SEM/EDS). Geochemical analysis was performed by X-ray fluorescence (XRF) Spectroscopy and Laser Ablation-Induced Coupled Plasma Mass Spectrometry (LA-ICPMS) techniques. The structural and morphological development of kaolinite in the outcropped shale samples of Mamu Formation is due to mechanical disintegration during transportation and re-deposition. Major oxides such as  $\text{SiO}_2$ ,  $\text{Al}_2\text{O}_3$  and  $\text{Fe}_2\text{O}_3$  constitute greater than 86% of the bulk composition. The weathering indices suggest highly weathered source materials. The plot of Cr versus Ni indicated the studied samples are Late Archean shale. Binary plots of trace elements suggest derivation from acidic or felsic sources rather than intermediate or basic source rocks. Ternary plot of  $\text{Na}_2\text{O} + \text{K}_2\text{O}$ ,  $\text{SiO}_2/10$  and  $\text{CaO} + \text{MgO}$  indicated multiple sources such as felsic igneous rocks or recycled residues of quartz-rich. Tectonic discrimination diagram depict a typical Passive Margin field.

**Keywords:** mineralogy, geochemistry, provenance, tectonic-setting, depositional history, formation

## **1. Introduction**

The Mamu Formation (Middle-Upper Maastrichtian) in the Anambra Basin is categorized by fossiliferous dark gray, indurated, and fissile shale. In addition, it is typically overlain by the intercalation of sand and shale facies sequence with coal inter-beds previously deposited under surface marine settings [1]. Selected studies have examined the Mamu Formation, Anambra Basin based on the following; stratigraphic/biostratigraphy [2–5], sedimentology and depositional environments [6], sequence stratigraphy [7, 8], palynology [1, 9–11], coal characterization [12–14], petroleum potential [15–17], palynofacies and kerogen analysis [18], geochemical indicator [19–21] and ichnology and lithofacies [22].

Some authors have indicated that analysis of the major elemental geochemistry of sedimentary rocks is useful in discerning its tectonic background [23, 24]. However, trace elements such as; La, Y, Sc, Cr, Th, Zr, Hf and Nb, mostly combined with TiO<sub>2</sub> are suitable for determining the provenance and tectonic settings. This is attributed to the comparatively poor mobility throughout sedimentary deposition and short habitation periods in seawater [25, 26]. The study by Armstrong-Altrin et al. [25] reported that all sedimentary rocks principally derived from Precambrian terrains could be predisposed to variations from the source materials. The comparative distribution of immovable elements showed diverse concentrations in felsic and basic rocks. For example, the immobile elements La and Th (enriched in felsic rocks) and Sc, Cr, and Co (basic rock compared to felsic rock enriched) are employed to understand the relative contributions of felsic and basic origins in shales derived from diverse tectonic locations [27, 28]. Akinyemi et al. [19] reported the paleoenvironment reconstruction of the outcropped Maastrichtian shale along Auchi-Igarra road using redox sensitive inorganic elements and mineralogical approach. However, the provenance, tectonic setting and paleoweathering of the Maastrichtian Mamu Shale Formation exposed at Auchi-Igarra Road, Edo State in Nigeria is hitherto not documented in the literature. Therefore, the main objective of the present study is to identify the source rock characteristics (i.e. provenance), source area weathering, and tectonic background through primary and immobile trace elements.

## **2. Geological setting**

The Anambra Basin is located from longitudes 6.30 E to 8.00 E and from the latitudes 5.00 N to 8.00 N. It is a syncline that trends from NE to SW as part of Central African Rift System. The basin was established in reaction to the widening and settling of major crustal blocks through the Early Cretaceous plate partitioning of South America and Africa [29]. The movements were restarted through additional activity on the Lower Tertiary plate subsequent to the alternation in the Upper Cretaceous rift. The proposed rift model was based on the evidence gathered by geomorphic, stratigraphic, structural, and paleontological research in literature [30–32]. The development of the basin denotes the third evolutionary sequence of the Benue Trough and its related basins when the Abakaliki Trough was elevated to the Abakaliki Anticlinorium whereas the Anambra Platform was transformed into the Anambra Basin [33, 34]. This transformation gave way to the westward transposition of the depositional axis of the troughs.

The sedimentation trend of the Anambra Basin is categorized by unstable depocentres. The basin consists of nearly 6 km of dense Cretaceous/Tertiary sediments

and is the structural connection from the Cretaceous Benue Trough to the Tertiary Niger Delta [35]. The basin is a portion of the lower Benue Trough comprising the post-deformational Campanian—Maastrichtian to the Eocene sedimentary strata. Sedimentation in the basin started with the Campano—Maastrichtian marine and paralic shales of the Enugu and Nkporo formations superimposed by the coal seams of the Mamu Formation. The fluivo-deltaic sandstones of the Ajali and Owelli sandstones are located in the Mamu Formation, which mostly comprises of its equivalents. The marine shales of the Imo and Nsukka formations were deposited in the Paleocene; superimposed by the tidal Nanka sandstones of the Eocene age. The downdip towards the Niger Delta, Akata Shale and Agbada Formation account for the Paleogene equivalents of the Anambra Basin [1].

### 3. Materials and method

#### 3.1 Sampling method

The outcrop of the Maastrichtian shale is located at coordinates 07°05'.071" N and 06°14'.826" E at 162.72 m above sea level (**Figure 1**). About 500 g of each sample was obtained at a sequence interval of 0.2 m from the shale. After collection, the samples directly stored in zipped lock polyethene bags for preservation at ambient temperatures. Next, the shales were oven dried at 60°C for 12 h. On cooling, the each sample was milled into a homogeneous powder using an agate ball mill. Next, the crushed shales characterized by scanning electron microscopy/energy dispersive spectroscopy (SEM/EDS) technique. Geochemical analysis was performed by X-ray fluorescence (XRF) Spectroscopy and Laser Ablation-Induced Coupled Plasma Mass Spectrometry (LA-ICPMS).

#### 3.2 X-ray diffraction analysis

The nine representative samples collected from the Maastrichtian shale of Mamu Formation were characterized to determine bulk mineralogy by X-ray diffraction (XRD). A detailed analytical procedure is reported in Akinyemi et al. [19].



**Figure 1.**  
Map showing the location of the study area.

### **3.3 SEM/EDS analysis**

The surface morphology of the nine samples was determined by scanning electron microscopy (SEM). The SEM is an FEI Nova NanoSEM (Model: Nova NanoSEM 230). The EDS analyses were determined at 20 kV and 5 mm working distance. The EDS detector is an Oxford X-Max (large area silicon drift detector) operated with the INCA- (INCAmicaF+ electronics and INCA Feature particle) analysis software.

### **3.4 XRF and LA-ICPMS analyses**

The composition of the metal oxides in the nine samples acquired at various heights in the Formation was determined by X-ray fluorescence (XRF) spectroscopy. The major oxides detected during XRF were; SiO<sub>2</sub>, TiO<sub>2</sub>, Al<sub>2</sub>O<sub>3</sub>, Fe<sub>2</sub>O<sub>3</sub>, MgO, MnO, CaO, Na<sub>2</sub>O, K<sub>2</sub>O, Cr<sub>2</sub>O<sub>3</sub> and P<sub>2</sub>O<sub>5</sub>. However, the composition of the trace elements in the samples was examined by LA-ICP-MS. The trace elements determined include; Ni, Cu, Zn, Ga, Rb, Sr, Y, Zr, Nb, Co, V, Pb, Th, U, Ti, Cr, Ba, La, Ce, Nd and P). The XRF and LA-ICP-MS tests were performed at the elemental analysis laboratories of the Stellenbosch University in South Africa. The techniques for sample preparation and ICP-MS analyses are as described in Akinyemi et al. [19]. The precision of the findings is presented as comparative standard deviation (in %) which is 5% for most of the elements analyzed with the LA-ICP-MS technique. The geochemical results from XRF were regularized to 100% volatile-free before plotting the data.

### **3.5 Loss on ignition determination**

The loss of ignition (LOI) was examined through the experimental techniques reported in Ojo [36]. The LOI was determined by first weighing an empty porcelain crucible, before adding 1 g of the dry mass of each sample to the crucible. Next, each sample was oven dried at 120°C for half an hour (30 min). The crucible and the sample were subsequently transferred to a furnace pre-heated to 1000°C for about 45 min. On completion, the samples were cooled in desiccators and weighed repeated until a constant weight was reached.

## **4. Results and discussion**

### **4.1 Mineralogy and surface morphology**

The base of the Mamu Formation is mainly dominated by quartz and kaolinite with minor traces of hematite, as described in literature [19]. The hematite in the base of the shale profile shows the oxidizing diagenetic setting for deposition. However, the upper portion of the profile is characterized by quartz and kaolinite with minor quantities of halloysite and grossite. **Figures 2** and **3** present the results of the SEM micrographs of the samples taken at the basal and upper part of the lithosection of the outcropped Mamu Shale.

The SEM investigation of samples taken at the basal and the upper part of the outcropped shale section show a mixture of sizes and morphologies of kaolinite in all the samples. As shown in **Figure 2a**, the quartz particles are spherical to rounded and exfoliated. The kaolinic particles are rolled with rough edges and some individual particles have lamellar shape indicating a terrigenous origin (**Figure 2b** and **c**).

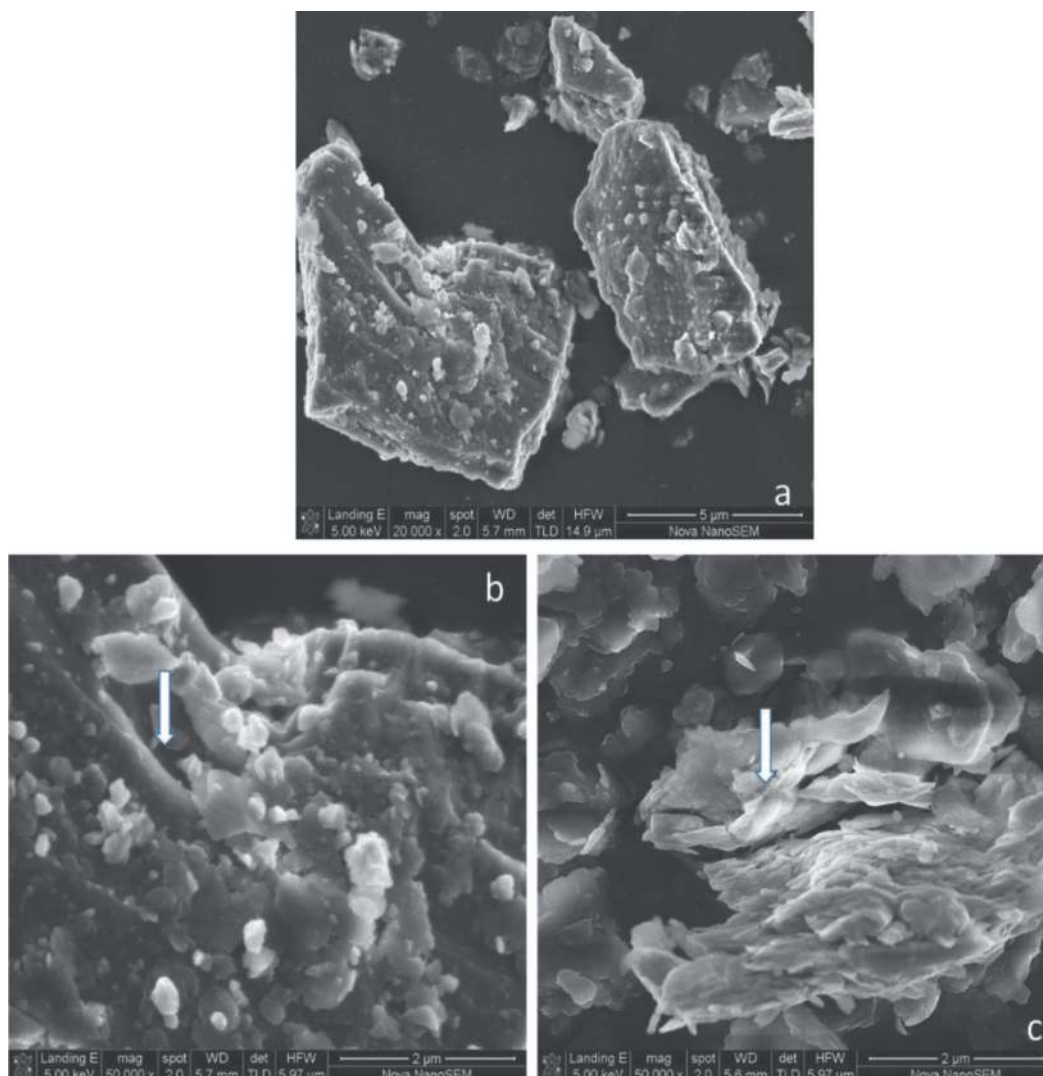


**Figure 2.** SEM photomicrographs of samples taken at basal part of outcropped shale of Mamu Formation. (a) Spherical quartz particle, rounded corners, and exfoliation, (b) rolled and rough edged kaolinite particles and (c) lamellar kaolinitic crystals.

Bortnikov et al. [37], reported that terrigenous kaolinite consists of lamellar particles and remains of differently preserved vermicular crystals. Kaolinite particles are arranged face to face and individuals show well defined crystalline pseudo-hexagonal and rough edges indicating detrital origin (**Figure 3b** and **c**). **Figure 3c** shows the face to face arrangement patterns of kaolinite particles in which larger platelets are surrounded by smaller ones suggesting bimodal origin (i.e. both terrigenous and authigenic varieties). Therefore, structural, and morphological growth of kaolinite in the outcropped shale samples of Mamu Formation is attributed to mechanical disintegration during transportation and redeposition.

#### 4.2 Bulk composition and geochemical classification

The chemical composition and ratios of selected major oxides of the studied samples are shown in **Tables 1** and **2**, respectively. The major oxide components are  $\text{SiO}_2$ ,

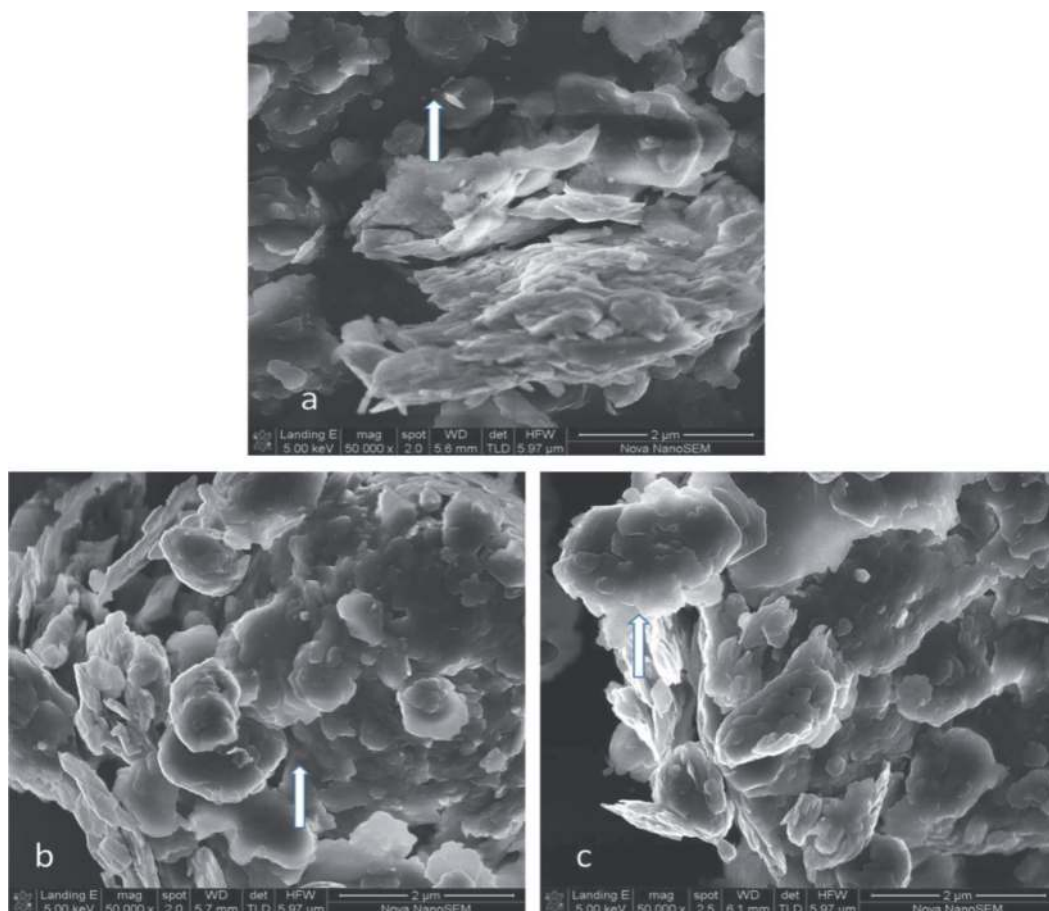


**Figure 3.**

SEM photomicrographs of samples taken at upper part of outcropped shale of Mamu Formation. (a) Authigenic quartz particle and face to face arrangement of kaolinite particles, (b) face to face arrangement patterns of larger platelets of kaolinite surrounded by smaller ones and (c) pseudo hexagonal and rough edges kaolinite particles.

$\text{Al}_2\text{O}_3$  and  $\text{Fe}_2\text{O}_3$  while other oxides occurred in minor quantities. The average contents of  $\text{SiO}_2$ ,  $\text{Al}_2\text{O}_3$  and  $\text{Fe}_2\text{O}_3$  are 64.84 wt%, 19.79 wt% and 2.22 wt%, respectively (**Table 1**). The ratios of  $\text{SiO}_2$  to  $\text{Al}_2\text{O}_3$  ranged between 1.96 wt.% and 26.95 wt.% with an average value of 5.29 wt.%. The  $\text{TiO}_2/\text{Al}_2\text{O}_3$  ratios varied between 0.04 and 0.08 with an average value of 0.07. The  $\text{K}_2\text{O}/\text{Na}_2\text{O}$  ratios ranged from 1.96 to 24.67 with an average value of 16.50 (**Table 2**). The ratios of  $\text{Fe}_2\text{O}_3 + \text{MgO}$  to  $\text{K}_2\text{O} + \text{Na}_2\text{O}$  ranged from 1.57 to 14.31 with an average value of 3.31. The plot of  $\log(\text{SiO}_2/\text{Al}_2\text{O}_3)$  versus  $\log(\text{Fe}_2\text{O}_3/\text{K}_2\text{O})$ , based on Herron [42], clearly shows the studied samples majorly fall within the shale field with one sample within the greywacke field and another in the Fe-sand field (**Figure 4**). This exceptional trend of the two samples is attributed to the relatively high  $\text{Fe}_2\text{O}_3$  contents in samples taken at 0.0 m and 0.2 m depths.

The major oxides were compared with the average values of shales worldwide [43], Average North American Shale [44, 45], Average Post-Archaean Australian Shale, and Upper Crust (data from Taylor and McLennan [46]). As observed, the average  $\text{SiO}_2$ ,  $\text{Al}_2\text{O}_3$ , and  $\text{TiO}_2$  in the studied samples is higher than Average World Shale, PAAS, NASC, Upper Crust [45]. Conversely, the average  $\text{Fe}_2\text{O}_3$ ,  $\text{CaO}$ ,  $\text{MgO}$ ,  $\text{MnO}$ ,  $\text{Na}_2\text{O}$ ,  $\text{P}_2\text{O}_5$  and  $\text{K}_2\text{O}$  contents in the studied samples is below the Average World Shale, PAAS, NASC, Upper Crust (**Table 3**) [45]. The average trace element such as Ba, Cu, Ni, Zn, and U in the studied samples is lower than shales from various regions of the globe

Sample ID	SiO <sub>2</sub>	Al <sub>2</sub> O <sub>3</sub>	CaO	Cr <sub>2</sub> O <sub>3</sub>	Fe <sub>2</sub> O <sub>3</sub>	K <sub>2</sub> O	MgO	MnO	Na <sub>2</sub> O	P <sub>2</sub> O <sub>5</sub>	TiO <sub>2</sub>	LOI	Total
0.0 m	92.20	3.42	0.08	0.00	3.15	0.15	0.10	0.00	0.08	0.10	0.29	1.81	101.37
0.2 m	63.62	19.56	0.02	0.02	3.56	1.00	0.25	0.01	0.10	0.11	1.42	10.79	100.45
0.4 m	62.48	21.49	0.02	0.02	1.56	1.07	0.27	0.01	0.06	0.09	1.57	11.15	99.77
0.6 m	72.77	14.83	0.04	0.01	2.75	0.74	0.21	0.01	0.08	0.10	1.09	7.917	100.53
0.8 m	51.83	26.46	0.06	0.03	2.26	1.41	0.35	0.01	0.07	0.17	1.10	16.16	99.9
1.0 m	61.22	23.25	0.02	0.02	1.62	1.00	0.22	0.01	0.06	0.07	1.55	11.52	100.56
1.4 m	56.52	24.86	0.04	0.02	1.94	1.20	0.29	0.01	0.06	0.12	1.33	13.84	100.23
1.6 m	64.49	20.01	0.04	0.02	1.46	0.97	0.22	0.00	0.05	0.08	1.61	10.45	99.39
1.8 m	58.30	24.20	0.06	0.02	1.66	1.19	0.29	0.00	0.05	0.06	1.40	12.68	99.39
2.0 m	58.27	24.22	0.07	0.02	1.67	1.20	0.30	0.00	0.05	0.07	1.41	12.7	99.97
Aver.	64.82	19.79	0.04	0.02	2.22	0.97	0.24	0.01	0.07	0.10	1.26	10.704	100.24

**Table 1.**  
 Bulk chemical composition of Maastrichtian Mamu shale sequence.

Sample ID	SiO <sub>2</sub> /Al <sub>2</sub> O <sub>3</sub>	TiO <sub>2</sub> /Al <sub>2</sub> O <sub>3</sub>	K <sub>2</sub> O/Na <sub>2</sub> O	Fe <sub>2</sub> O <sub>3</sub> + MgO/K <sub>2</sub> O + Na <sub>2</sub> O	CIA	CIW	PIA	MIA
0.0 m	26.95	0.08	1.96	14.31	91.75	95.60	95.40	91.19
0.2 m	3.25	0.07	10.05	3.47	94.60	99.40	99.37	98.80
0.4 m	2.91	0.07	17.97	1.62	94.95	99.64	99.62	99.28
0.6 m	4.91	0.07	9.41	3.62	94.54	99.21	99.17	98.42
0.8 m	1.96	0.04	21.53	1.78	94.53	99.53	99.50	99.06
1.0 m	2.63	0.07	16.90	1.74	95.57	99.67	99.65	99.34
1.4 m	2.27	0.05	19.33	1.76	95.01	99.59	99.57	99.19
1.6 m	3.22	0.08	19.37	1.66	95.01	99.57	99.55	99.14
1.8 m	2.41	0.06	23.80	1.57	94.90	99.55	99.52	99.10
2.0 m	2.41	0.06	24.67	1.58	94.84	99.51	99.48	99.01
Aver.	5.29	0.07	16.50	3.31	94.57	99.13	99.08	98.25

$CIA = 100 \cdot Al_2O_3 / (Al_2O_3 + CaO + Na_2O + K_2O)$  [38].  
 $CIW = (Al_2O_3 / (Al_2O_3 + CaO + Na_2O)) \cdot 100$  [39].  
 $PIA = (Al_2O_3 - K_2O) / (Al_2O_3 + CaO + Na_2O - K_2O) \cdot 100$  [40].  
 $MIA = 2 \cdot (CIA - 50)$  [41].

**Table 2.**  
Ratios of major oxides in the Maastrichtian Mamu shale sequence.



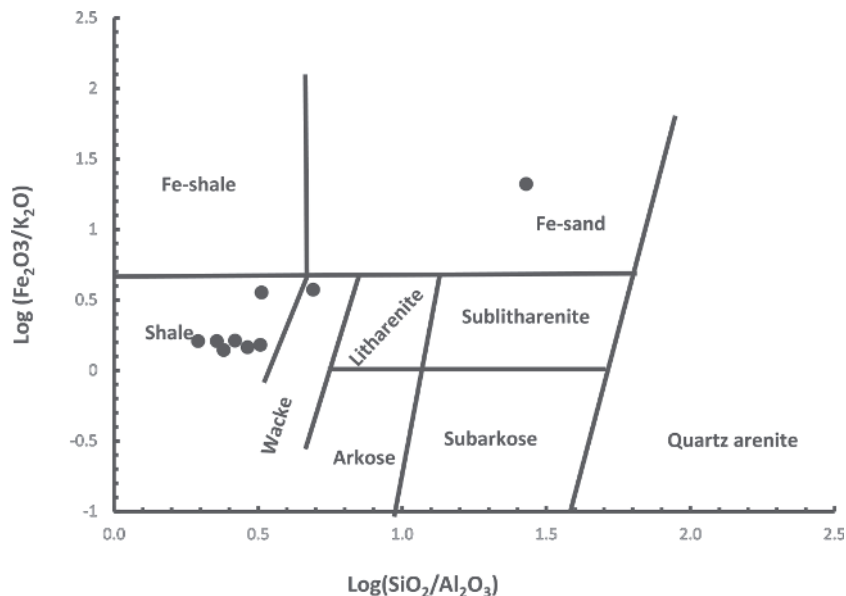


**Figure 4.** Chemical classification of the Mamu shale sequence based on  $\log (SiO_2/Al_2O_3)$  vs.  $\log (Fe_2O_3/K_2O)$  diagram of Herron [42].

Oxides	Present study	AWS	PAAS	NASC	UC	Turekan and Wedephol [47]
SiO <sub>2</sub>	64.17	58.90	62.80	64.80	66.00	58.5
Al <sub>2</sub> O <sub>3</sub>	20.23	16.70	18.90	16.90	15.20	15
Fe <sub>2</sub> O <sub>3</sub>	2.16	6.90	7.22	5.65	5.00	4.72
TiO <sub>2</sub>	1.28	0.78	1.00	0.70	0.50	0.77
CaO	0.04	2.20	1.30	3.63	4.20	3.1
Cr <sub>2</sub> O <sub>3</sub>	0.02	—	—	—	—	—
K <sub>2</sub> O	0.99	3.600	3.700	3.970	3.400	3.1
MgO	0.24	2.60	2.20	2.86	2.20	2.5
MnO	0.01	—	0.11	0.06	0.08	—
Na <sub>2</sub> O	0.07	1.60	1.20	1.14	3.90	1.3
P <sub>2</sub> O <sub>5</sub>	0.10	—	0.16	0.13	—	0.16
LOI	10.90	—	6.00	—	—	—
H <sub>2</sub> O <sup>-</sup>	—	—	—	—	—	—
Total	100.16	93.28	104.59	99.84	100.48	89.15

Average Shale Worldwide [43]; Average Post-Archaean Australian Shale [48]; NASC = Average North American Shale (data from [44]); UC = Upper Crust (data from [48]); Turekan and Wedephol [47].

**Table 3.** Major oxides of Maastrichtian Mamu shale sequence compared with worldwide shales.

(Table 4). On the other hand, the average concentrations of Ce, Co, Nb, Rb, Sr, V, Y, Zr, Th, Cr, La and Nd in the studied samples is higher than shales from various areas of the globe (Table 4).

Trace elements	Present study	ASW	*PAAS	*NASC	UC	Turekan and Wedephol [47]
As	—	—	—	28.4	1.50	—
Ba	245.8	580	650	636		580
Ce	183.0	—	80	66.7	64	—
Co	54.3	19	23	25.7	10	—
Cu	11.0	45	50	—	25	45
Nb	26.7	—	19	13	25	—
Ni	16.2	68	55	58	20	68
Pb	150.9	22	20	—	—	—
Rb	52.4	140	160	125	112	—
Sr	95.7	300	200	142	350	300
V	212.7	130	150	130	60	130
Y	47.8	—	25	35	22	—
Zn	27.4	95	85	—	71	95
Zr	328.9	160	210	200	190	160
Ga	25.0	—	—	—		—
Th	15.1	—	14.6	12.3	10.7	—
U	0.7	3.7	3.1	2.66	2.8	—
Ti	9475.0	—	—	—	—	—
Cr	138.8	90	110	125	35.0	—
La	72.0	—	38	31.1	30	—
Nd	77.8	—	32	27.4	26	—
P	450.4	—	—	—	—	—

*Average Shale Worldwide [43]; Average Post-Archaean Australian Shale [48]; NASC = Average North American Shale (data from [44]); UC = Upper Crust (data from [48]); Turekan and Wedephol [47].*

**Table 4.**  
Comparison of average trace element contents with other worldwide shales.

### 4.3 Source area weathering

Several authors have recommended that the chemical composition of clastic sedimentary rocks is mainly reliant on the composition and weathering settings in the area of the source rock [49, 50]. The study by Nesbitt and Young [50] examined the extent of weathering of a clastic sedimentary rock by computing the chemical index alteration (CIA) which is defined as:

$$CIA = 100 \times \left( \frac{Al_2O_3}{Al_2O_3 + CaO^* + Na_2O + K_2O} \right) \quad (1)$$

This weathering index is mostly valid when Ca, Na, and K declines with increasing weathering intensity [51]. In Eq. (1), CaO\* is the concentration of CaO fused in the silicate portion of the shales examined [40]. However, the CaO correction from

the carbonate influence was not performed for the samples examined in this study due to lack of CO<sub>2</sub> data. Therefore, the computation for CaO\* from the silicate portion requires adopting Bock et al. [52] hypothesis. Based on the assumption, the CaO values are only valid when CaO ≤ Na<sub>2</sub>O. However, if CaO > Na<sub>2</sub>O, it is probable that the CaO concentration is equivalent to Na<sub>2</sub>O [52]. The outlined technique is the basis for the measure of the weathering intensity and the ratio of the lesser aluminous compound to feldspar [53]. The Chemical Index of Weathering (CIW) proposed by Harnois [39] is similar to the CIA except for the exclusion of K<sub>2</sub>O in the equation:

$$CIW = \text{molar} \times \left( \frac{Al_2O_3}{Al_2O_3 + CaO + Na_2O} \right) \quad (2)$$

For CIA and CIW, the values are deduced in the similar to the unweathered upper continental crust (~50) and for greatly weathered constituents (~100) with comprehensive elimination of the alkali and alkaline-earth metals [26, 54, 55]. Typically, small values of CIA (50 or less) may reflect cool and/or dry conditions [40]. In this study, the values of CIA for shale samples ranged from 91.75% to 95.57%, or 94.57% on average. Similarly, the values of CIW varied between 95.60% and 99.67%, or 99.13% on average. The CIA and CIW standards for the examined shale sequence indicate highly weathered source constituents. This observation is corroborated by the previous study by Ejeh [20].

The chemical weathering intensity is typically computed according to the Plagioclase Index of Alteration [40] in molecular proportions:

$$PIA = \text{molar} \times \left( \frac{Al_2O_3 + K_2O}{Al_2O_3 + CaO^* + Na_2O - K_2O} \right) \times 100 \quad (3)$$

The term CaO\* represents the CaO residing exclusively in the silicate portion. The unweathered plagioclase typically has a PIA value of 50. In this study, the PIA for the shale samples ranged from 95.40% to 99.67% with an average value of 99.08%, which indicates highly weathered source constituents.

The Mineralogical Index of Alteration (MIA) is a weathering index computed from the equation [41];

$$PIA = 2 \times (CIA - 50) \quad (4)$$

The MIA values from 0 to 20% are designated as incipient i.e. just starting, 20–40% (weak), 40–60% (moderate), and 60–100% as strong to a great degree of weathering. The MIA values for shale samples examined ranged from 91.19% to 99.34%, with an average value of 98.25%. Therefore, the MIA for shales showed a great amount of source weathering constituents.

**Figure 5** shows that the studied samples plots are near the “A” vertex above the upper continental crust (UCC) line, which indicates a high extent of weathering. Nesbitt et al. [49] used the ternary diagrams of Al<sub>2</sub>O<sub>3</sub>-(CaO + Na<sub>2</sub>O)-K<sub>2</sub>O (the A-CN-K), and Fe<sub>2</sub>O<sub>3</sub> + MgO-(CaO + Na<sub>2</sub>O + K<sub>2</sub>O)-Al<sub>2</sub>O<sub>3</sub> (the A-CNK-FM) to deduce weathering trends. On both the A-CN-K and the A-CNK-FM diagrams in **Figures 6** and **7** respectively, all the sediments indicated an extreme weathering history. The studied samples plot evidently suggest different contents of Al<sub>2</sub>O<sub>3</sub>, CaO, Na<sub>2</sub>O, and K<sub>2</sub>O in a region examined compared to the Average World Shale, PAAS, NASC, and UC indices. The studied samples plot near the high contents of Al<sub>2</sub>O<sub>3</sub> suggests a relatively high intensity of

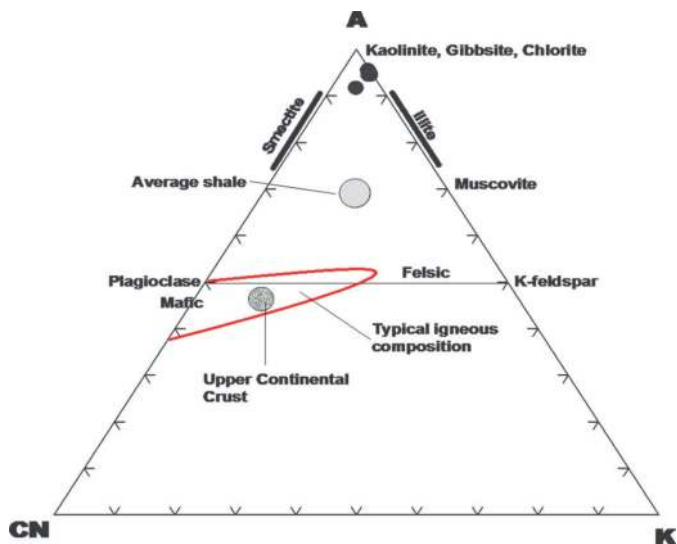


**Figure 5.** Ternary diagram showing the weathering trend of the studied samples (all in molar proportions);  $Al_2O_3$ - $CaO + Na_2O$ - $K_2O$  (A-CN-K). Fields from Gu et al. [56].

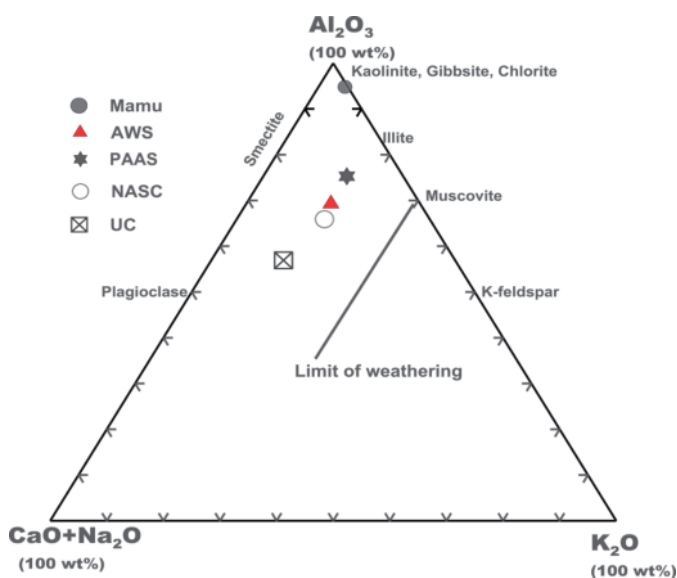


**Figure 6.**  $Al_2O_3$ - $(CaO + Na_2O)$ - $K_2O$  plot of sediment samples (after [49, 50]), compared to data for post-Archean average shale (PAAS) and upper crust (UC) given by Taylor and McLennan [48]; and north American shale composite (NASC) given by Gromet et al. [44].

weathering. This implies that substantial content of the alkali and alkaline earth elements were detached from the shales in this study [57].

#### 4.4 Chemical maturity and paleoclimatic condition

Suttner and Dutta [58], suggested the plot of  $SiO_2$  versus  $Al_2O_3 + K_2O + Na_2O$  to infer the paleoclimatic condition of the source region. The studied samples mainly fall within the semi-arid condition at the source area (Figure 8). Therefore, the prevalent dry settings of the source region will slow down the weathering process and thereby impede chemical maturity.

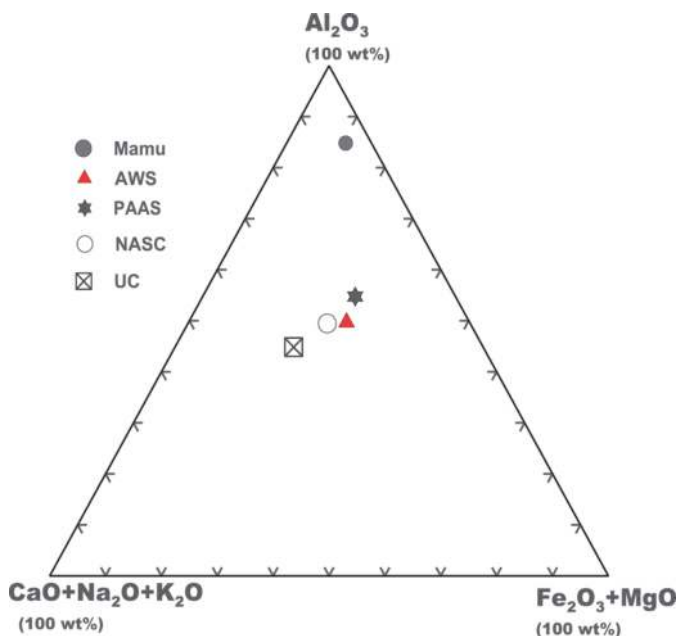


**Figure 7.** Triangular  $Al_2O_3$ - $(CaO + Na_2O + K_2O)$ - $Fe_2O_3 + MgO$  plot of the current sediment data (after [49, 50]) in comparison with post-Archean average shale and upper crust (data from [48]) and north American shale composite (data from [44]).

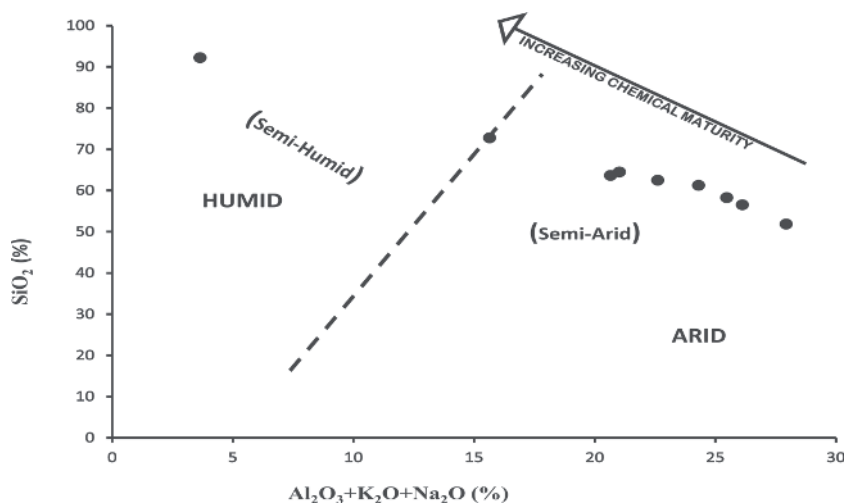


**Figure 8.** Chemical maturity and paleoclimate of the Mamu shale sequence expressed by bivariate plot of  $SiO_2$  versus  $Al_2O_3 + K_2O + Na_2O$  (after [58]).

#### 4.5 Provenance

Major element geochemistry could offer empirical evidence on the rock composition, source rock, along with the outcome of sedimentary techniques like sorting and weathering [26]. The outlined properties provide evidence of the source rock attributes and definite patterns of historical sediments [59, 60]. Therefore, it is a common practice to infer the origin of deposits and sedimentary rocks [61–66]. The two variable plots of  $Na_2O$  versus  $K_2O$  reveals the studied samples are rich in quartz, which shows felsic sources (Figure 9). The ternary diagram shows the plots of the

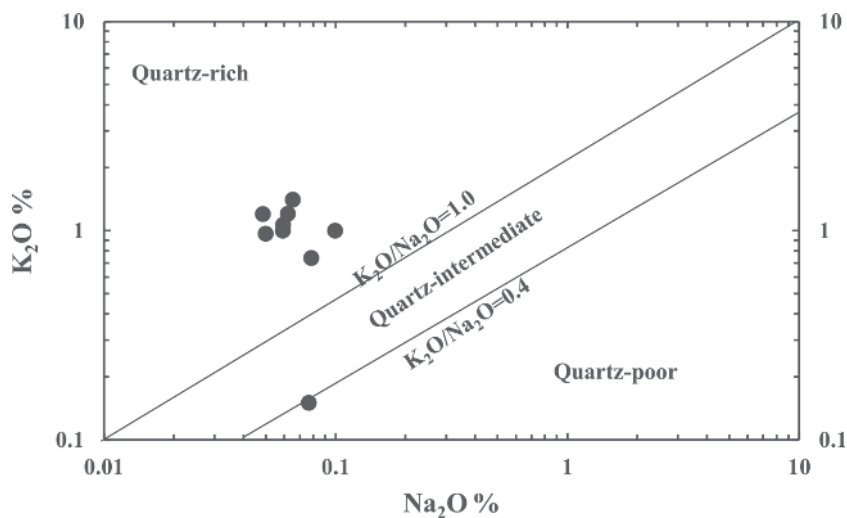


**Figure 9.** Bivariate plot of  $\text{Na}_2\text{O}$  versus  $\text{K}_2\text{O}$  of the Mamu shale sequence showing quartz content, after Crook [67].

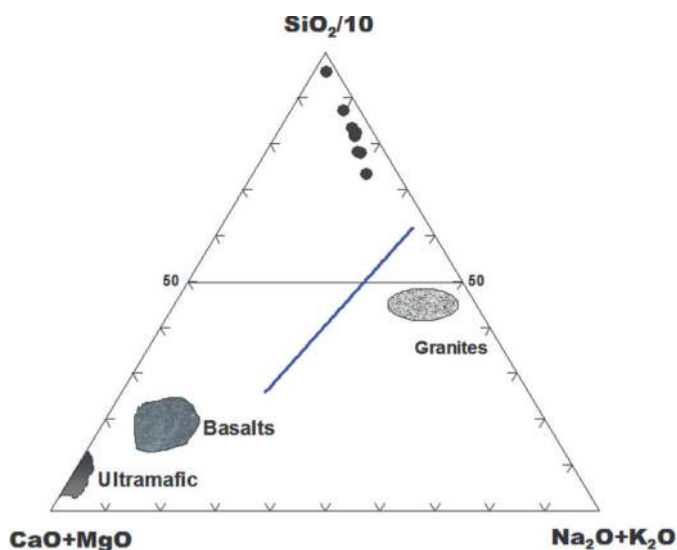


**Figure 10.** Plot of  $\text{Na}_2\text{O} + \text{K}_2\text{O}$ ,  $\text{SiO}_2/10$  and  $\text{CaO} + \text{MgO}$  to illustrate possible affinities of the samples to felsic, mafic, and ultramafic rocks (after [48]).

studied samples in the  $\text{SiO}_2$  are distant from the basalts, ultramafic, and granitic regions (**Figure 10**). This submits that the felsic igneous or metamorphic or recycled rocks rich in quartz deposits derivation are evident.

Similarly, the composition of zircon is used to describe the nature and content of source rock [68, 69]. The study by Hayashi et al. [68] recommended that  $\text{TiO}_2/\text{Zr}$  ratios can distinguish the three different felsic, intermediate, and mafic types of source rock. The  $\text{TiO}_2$  versus  $\text{Zr}$  plot (**Figure 11**) indicates that the samples examined are mostly plotted in the intermediate field although few lie within the felsic and mafic zones. The origins of a sedimentary rock suite can be computed through the  $\text{K}_2\text{O}$  versus  $\text{Rb}$  ratios, which are mostly identical to the standard Upper Continental Crust values [70]. The  $\text{Cr}/\text{V}-\text{Y}/\text{Ni}$  ratios could also provide estimations of the specific composition of chromium over other ferromagnesian elements [26, 71].

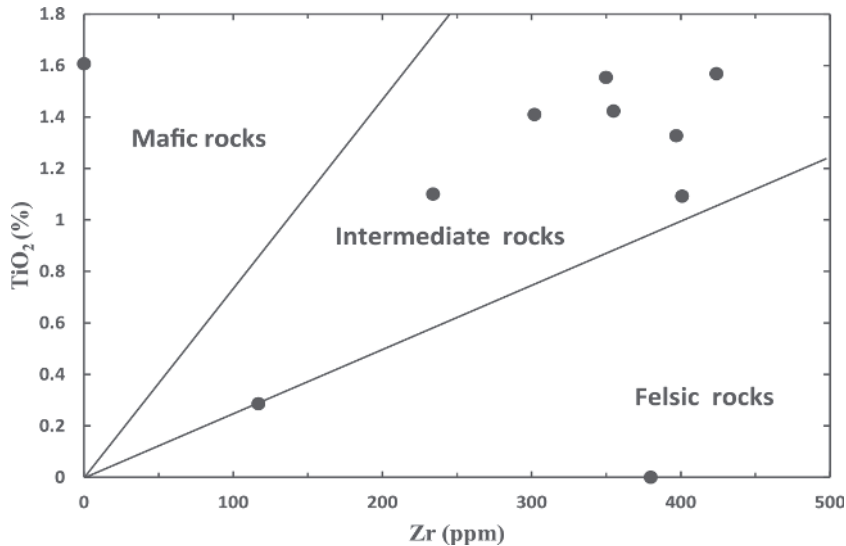


**Figure 11.**  
*TiO<sub>2</sub>-Zr plot for the Mamu shale sequence [68].*

**Figure 12** shows the plots of studied samples in the acidic/intermediate composition zone with one sample located in the basic composition zone. The Cr/V ratio describes the enrichment of Cr regarding additional ferromagnesian elements. However, the Y/Ni ratio appraises the connection amongst the ferromagnesian minor elements (denoted by Ni) and the HREE using Y as a substitute [26]. The Y/Ni ratios typically range across values from midway to the felsic calc-alkaline rocks (**Figure 13**). The sediments resulting from ultrabasic origins typically have high Cr/V ratios above 1 and low Y/Ni ratios below 1 [71]. The Cr/V ratio ranged from 0.52 to 0.99, or 0.66 on average. However, the Y/Ni ratio was from 1.1 to 9.6 with an average value of 4.79, which suggests felsic compositions in the source materials.

**Figure 14** reveals that the source rocks for shales examined are Late-Archean. The residues reveal minimal scatter along with trace Cr constituents, which indicates

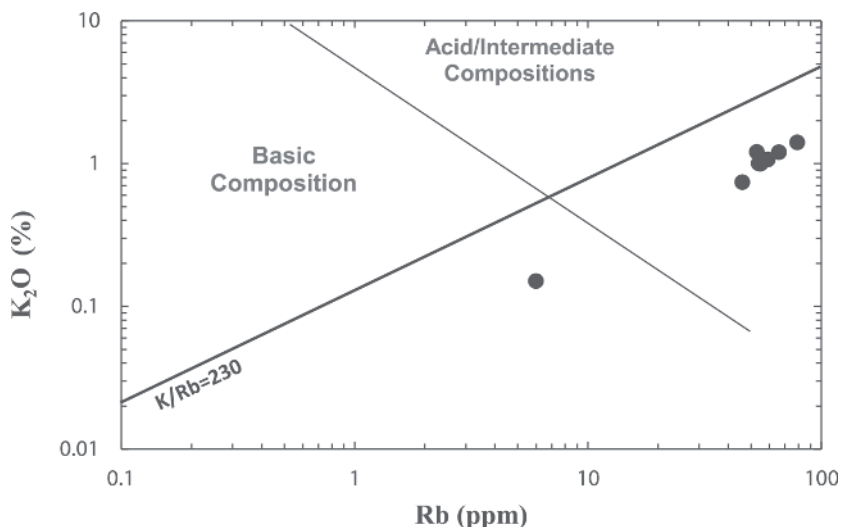


**Figure 12.**  
*K<sub>2</sub>O versus Rb plot. Fields after Floyd and Leveridge [72].*

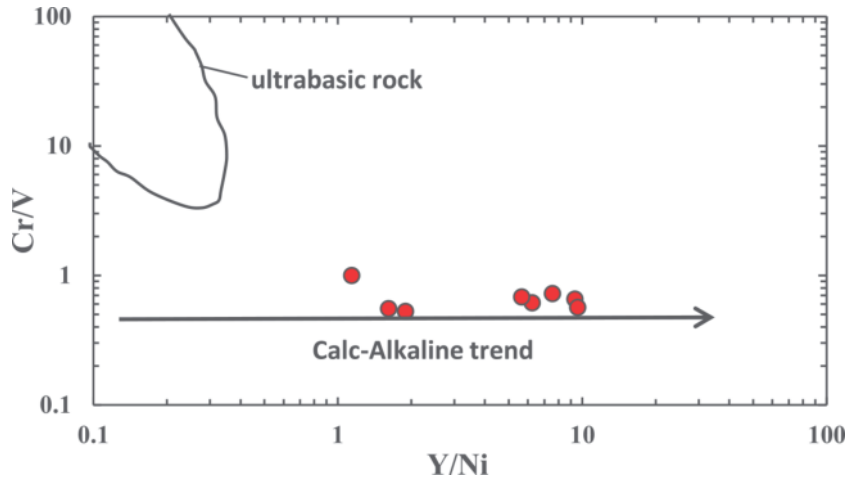


**Figure 13.** *Cr/V–Y/Ni plots for the sediments showing the lack of ultrabasic sources (after [26]). Ultrabasic field of sands derived from ultrabasic rocks, after Ortiz and Roser [73].*

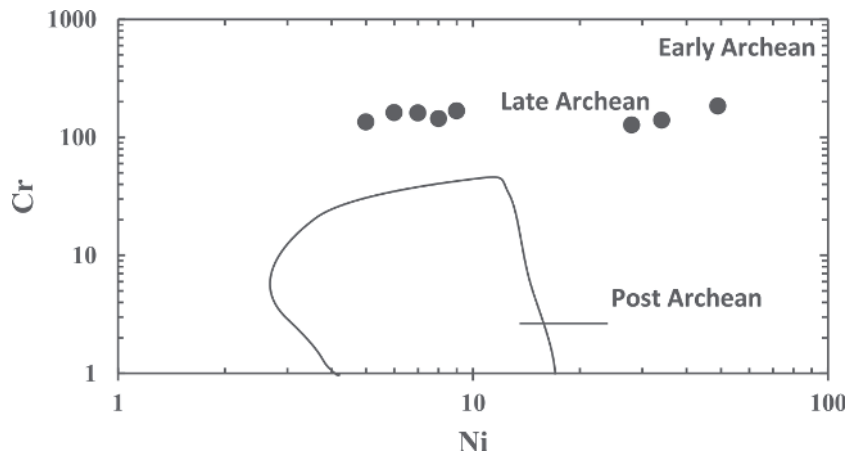


**Figure 14.** *Cr–Ni plot for the studied samples showing the plots in the late-Archean field [48] and fractionation from source rocks to the sediments.*

depletion and homogenization could have occurred in the course of transportation or weathering. Floyd et al. [70], applied immovable elements such as  $\text{TiO}_2$  and Ni to deduce the original lithological structure of rocks. The technique was also employed to separate unformed residues of magmatic origins from standard mature sediments. The studied samples are plotted within the zone of an acidic or felsic source (**Figure 15**). According to Cullers and Berendsen [74], the Th/Co versus La/Co ratios are used to distinguish the source materials of sedimentary rocks. The shale samples examined in this study are plotted mainly in the upper continental crust and one sample each show close proximity to basaltic and granodioritic zone respectively (**Figure 16**). This observation agreed with the previous study conducted by Ogbahon and Olujinmi [76].

#### 4.6 Tectonic evolution

The discrimination diagrams of major elements can be used to describe or distinguish rocks based on the tectonic setting was suggested by several authors [23, 24, 77].



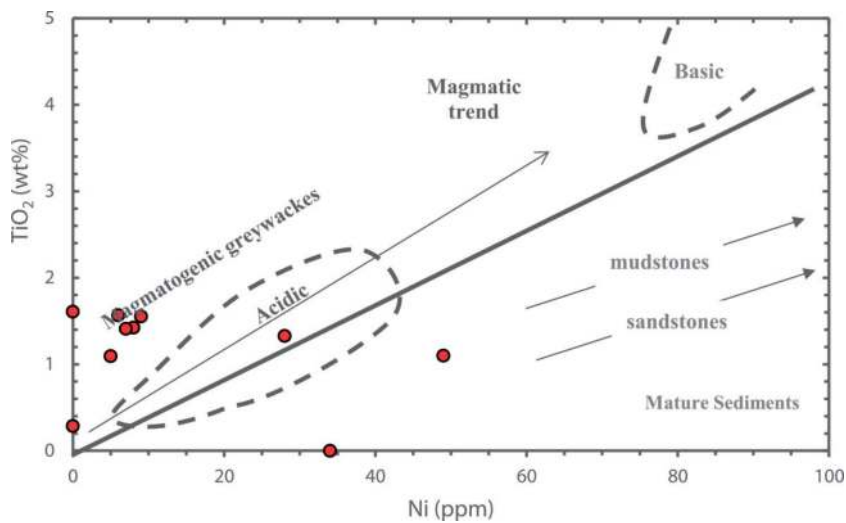


**Figure 15.**  
*TiO<sub>2</sub> vs. Ni plot. Fields and trends fashioned after Gu et al. [56] and Floyd et al. [70].*

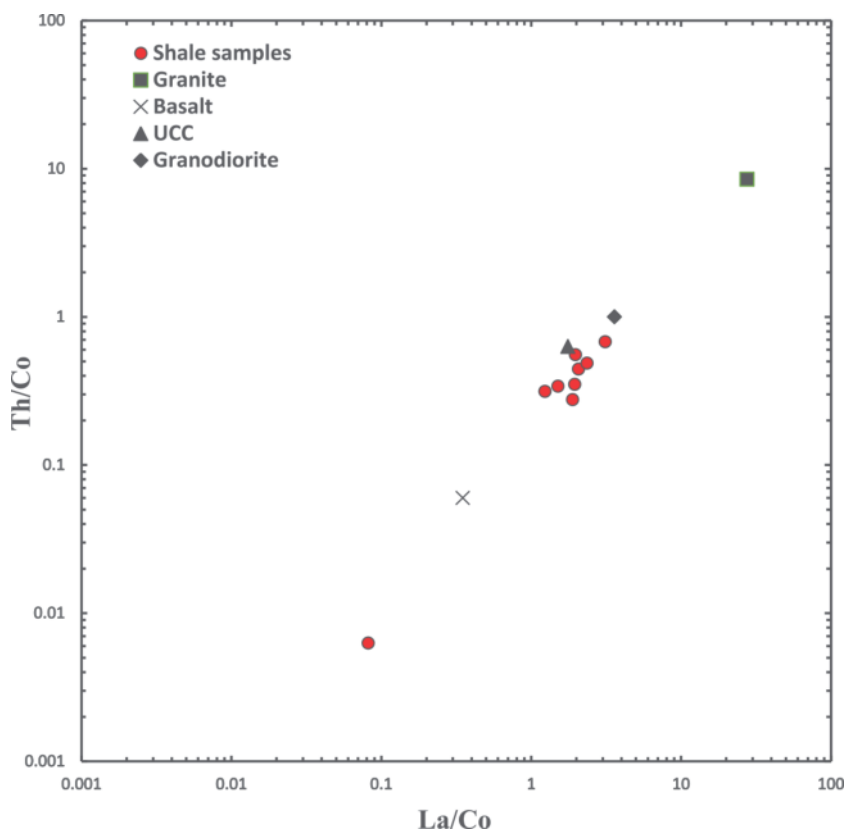


**Figure 16.**  
*Source rock discrimination diagram for Mamu shale sequence (after [74]), in relation to average values of granites, basalts, granodiorite [75] and upper continental crust [46, 48].*

Roser and Korsch [24] suggested four tectonic discrimination diagrams based on the SiO<sub>2</sub> as the x-axis and K<sub>2</sub>O/Na<sub>2</sub>O as the y-axis. As shown in **Figure 17**, the studied samples indicated Passive Margins tectonic field. Furthermore, the tectonic discrimination

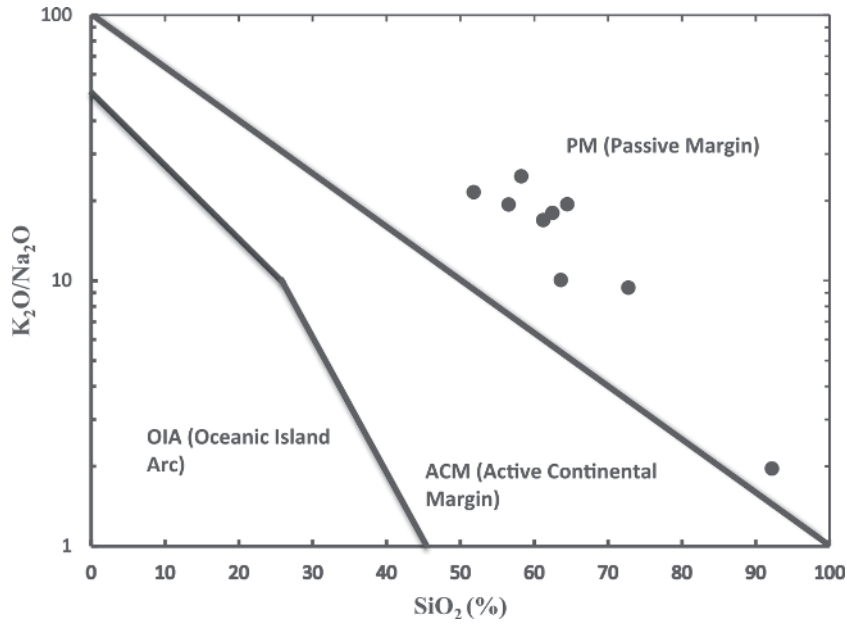


**Figure 17.** Tectonic discrimination plot for the Mamu shale sequence (after [24]).

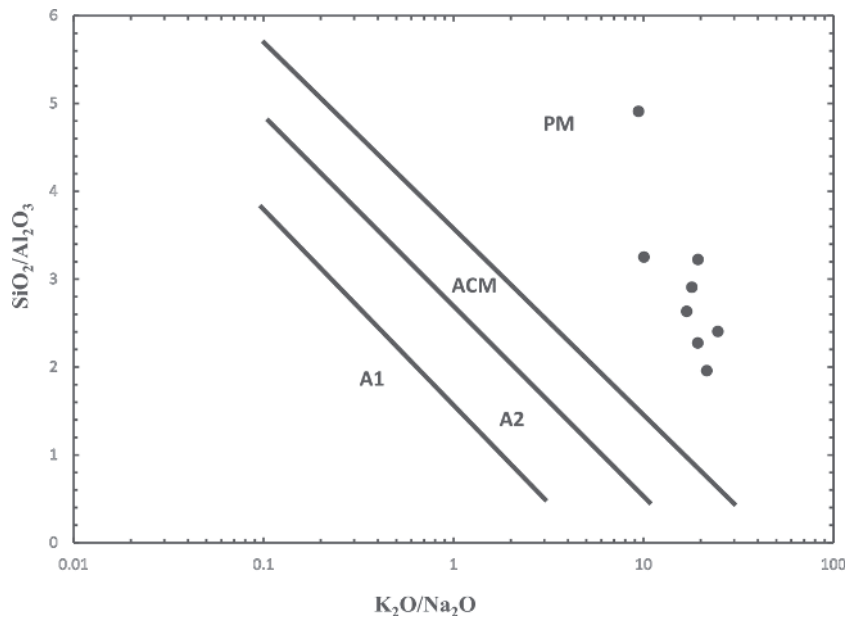


**Figure 18.**  $SiO_2/Al_2O_3$  ratio versus  $K_2O/Na_2O$  ratio plot for Mamu shale sequence. Fields and boundary lines (after Maynard et al. [78]; Roser and Korsch [24]). A1 = arc setting, basaltic and andesitic detritus; A2 = evolved arc setting; ACM = active continental margin; PM = passive margins.

diagram of  $K_2O/Na_2O$  as the x-axis and  $SiO_2/Al_2O_3$  as the y-axis similarly depicted studied samples in the Passive Margins zone (**Figure 18**). This trend is supported by the previous study done by Ogbahon and Olujinmi [76]. The residues from the passive margin are fundamentally rich in quartz and derived from established continental regions, placed in intracratonic basins or on passive continental boundaries [24].

## 5. Summary and conclusion

In this study, the structural and morphological evolution of kaolinite in the samples is attributed to mechanical disintegration during sediment transportation and redeposition. The shales of the Mamu Formation show considerable variation with regards to major oxides, trace, and rare earth elements. The abundant major oxides showed that  $\text{SiO}_2$ ,  $\text{Al}_2\text{O}_3$  and  $\text{Fe}_2\text{O}_3$  constitute more than 86% of the bulk chemical composition. The plot of  $\log (\text{SiO}_2/\text{Al}_2\text{O}_3)$  versus  $\log (\text{Fe}_2\text{O}_3/\text{K}_2\text{O})$  indicated that the samples examined are majorly within the shale field. The weathering indices such as CIA, CIW, PIA and MIA indicated highly weathered source materials. Provenance indicated heterogeneous sources for the studied clastic sediments. The examination of geochemical parameters such as Th/Co versus La/Co,  $\text{TiO}_2$  versus Ni, Cr/V versus Y/Ni and  $\text{TiO}_2$  versus Zr suggest the samples could be the result of acidic or felsic sources and not intermediate or basic source rocks. The Cr versus Ni plots indicated the studied samples are Late Archean shales. In the provenance discrimination diagrams based on major and immobile elements, the outcropped shale samples show geochemical markers in agreement with the source rocks of intermediate structure, whereas the tectonic discrimination diagrams indicate Passive Continental Margin field.

### Author details

Segun A. Akinyemi<sup>1\*</sup>, Olajide F. Adebayo<sup>1</sup>, Henry Y. Madukwe<sup>1</sup>,  
Adeyinka O. Aturamu<sup>1,2</sup> and Olusola A. OlaOlorun<sup>1</sup>


1 Geology Department, Ekiti State University, Ado Ekiti, Nigeria

2 Geology Department, University of Leicester, Leicester, UK

\*Address all correspondence to: [segun.akinyemi@eksu.edu.ng](mailto:segun.akinyemi@eksu.edu.ng)

### IntechOpen

---

© 2022 The Author(s). Licensee IntechOpen. This chapter is distributed under the terms of the Creative Commons Attribution License (<http://creativecommons.org/licenses/by/3.0>), which permits unrestricted use, distribution, and reproduction in any medium, provided the original work is properly cited. 

## References

- [1] Ogala J, Ola-Buraimo A, Akaegbobi I. Palynological and palaeoenvironmental study of the middle-upper Maastrichtian Mamu coal facies in Anambra Basin, Nigeria. *World Applied Sciences Journal*. 2009;7(12):1566-1575
- [2] Adeniran B. Maastrichtian tidal flat sequences from the northern Anambra Basin, southern Nigeria. *Nigerian Association of Petroleum Exploration Bulletin*. 1991;6:56-66
- [3] Gebhardt H. Benthic Foraminifera from the Maastrichtian lower Mamu Formation near Leru (southern Nigeria); paleoecology and paleogeographic significance. *The Journal of Foraminiferal Research*. 1998;28(1):76-89
- [4] Ladipo KO. Paleogeography, sedimentation and tectonics of the upper cretaceous Anambra Basin, southeastern Nigeria. *Journal of African Earth Sciences (and the Middle East)*. 1988;7(5-6):865-871
- [5] Petters S. Stratigraphic evolution of the Benue trough and its implications for the upper cretaceous paleogeography of West Africa. *The Journal of Geology*. 1978;86(3):311-322
- [6] Lukman A, Ayuba R, Alege T. Sedimentology and depositional environments of the Maastrichtian Mamu formation, northern Anambra Basin, Nigeria. *Advances in Applied Science Research*. 2020;9(2):53-68
- [7] Nwajide CS, Reijers TJ. Sequence architecture in outcrops: examples from the Anambra Basin, Nigeria. *NAPE Bulletin*. 1996;11(01):23-32
- [8] Onyekuru S, Iwuagwu C. Depositional environments and sequence stratigraphic interpretation of the Campano-Maastrichtian Nkporo shale group and Mamu formation exposures at Leru-Okigwe axis, Anambra Basin, Southeastern Nigeria. *Australian Journal of Basic Applied Sciences*. 2010;4(12):6623-6640
- [9] Mebradu S. Palynofacies of Enugu/Iva valley shales, Enugu State, Nigeria. *Journal of Mining & Geology*. 1982;26(1):5-11
- [10] Onuigbo E, JO, E.-E., & Okoro, A. Palynology, paleoenvironment and sequence stratigraphy of the Campanian-Maastrichtian deposits in the Anambra Basin, Southeastern Nigeria. *European Journal of Scientific Research*. 2012;78(3):333-348
- [11] Onyeachonam N, Fregene TJ. Palynological studies of upper Cretaceous-Paleocene rocks in Auchi sheet 266, Benin flank, Western extension of the Anambra Basin, southwestern Nigeria. *Journal of Geosciences and Geomatics*. 2021;9(3):145-159. DOI: 10.12691/jgg-9-3-5
- [12] Akande SO, Hoffknecht A, Erdtmann BD. Rank and petrographic composition of selected upper cretaceous and tertiary coals of southern Nigeria. *International Journal of Coal Geology*. 1992;20(3-4):209-224
- [13] Akinyemi SA, Adebayo OF, Madukwe HY, Kayode AT, Aturamu AO, OlaOlorun OA, et al. Elemental geochemistry and organic facies of selected cretaceous coals from the Benue trough basin in Nigeria: Implication for paleodepositional environments. *Marine and Petroleum Geology*. 2022;137:105490

- [14] Akinyemi SA, Adebayo OF, Nyakuma BB, Adegoke AK, Aturamu OA, OlaOlorun OA, et al. Petrology, physicochemical and thermal analyses of selected cretaceous coals from the Benue Trough Basin in Nigeria. *International Journal of Coal Science & Technology*. 2020;7(1):26-42
- [15] Maju-Oyovwikowhe GE, Malomi BP. Evaluation of hydrocarbon potential, quality of source rock facies, and delineating of their depositional environment in Mamu formation of Anambra Basin, Nigeria. *Journal of Applied Sciences & Environmental Management*. 2019;23(3):383-388
- [16] Ogala JE. Hydrocarbon potential of the upper cretaceous coal and shale units in the Anambra Basin, Southeastern Nigeria. *Petroleum & Coal*. 2011;53(1):35-44
- [17] Ogungbesan GO, Adedosu TA. Geochemical record for the depositional condition and petroleum potential of the late cretaceous Mamu formation in the western flank of Anambra Basin, Nigeria. *Green Energy & Environment*. 2020;5(1):83-96
- [18] Chiaghanam O, Chiadikobi K, Ikegwuonu O, Omoboriowo A, Onyemesili O, Acra E. Palynofacies and kerogen analysis of upper cretaceous (early Campanian to Maastrichtian) Enugu shale and Mamu formation in Anambra Basin, south-eastern Nigeria. *International Journal of Scientific & Technology Research*. 2013;2(8): 87-97
- [19] Akinyemi S, Adebayo O, Ojo O, Fadipe O, Gitari W. Mineralogy and geochemical appraisal of paleo-redox indicators in Maastrichtian outcrop shales of Mamu formation, Anambra Basin, Nigeria. *Journal of Natural Science Research*. 2013;3:48-64
- [20] Ejeh OI. Geochemistry of rocks (late cretaceous) in the Anambra Basin, SE Nigeria: Insights into provenance, tectonic setting, and other palaeo-conditions. *Heliyon*. 2021;7(10):e08110
- [21] Okiotor ME, Ighodaro EJ. Geochemical appraisal of the Mamu shales exposed around Igodor in the Benin flank of the Anambra Basin, Nigeria. *Journal of Applied Sciences & Environmental Management*. 2020;24(3):489-493
- [22] Odumodu CF. Ichnology and lithofacies analysis of the Campano-Maastrichtian Mamu formation in the northern parts of the Anambra Basin, Nigeria. *International Journal of Geology. Earth Environmental Sciences*. 2014;4:3
- [23] Bhatia MR. Plate tectonics and geochemical composition of sandstones. *The Journal of Geology*. 1983;91(6):611-627
- [24] Roser B, Korsch R. Determination of tectonic setting of sandstone-mudstone suites using content and ratio. *The Journal of Geology*. 1986;94(5):635-650
- [25] Armstrong-Altrin J, Lee YI, Verma SP, Ramasamy S. Geochemistry of sandstones from the upper Miocene Kudankulam Formation, southern India: Implications for provenance, weathering, and tectonic setting. *Journal of Sedimentary Research*. 2004;74(2):285-297
- [26] McLennan S, Hemming S, McDaniel D, Hanson G. Geochemical approaches to sedimentation, provenance, and tectonics. *Special Papers-Geological Society of America*. 1993:21-21. DOI: 10.1130/SPE284-p21
- [27] Condie KC, Wronkiewicz DJ. A new look at the Archaean-Proterozoic boundary sediments and the tectonic

setting constraint. *Developments in Precambrian Geology*. 1990;**8**:61-83

[28] Okunlola OA, Idowu O. The geochemistry of claystone-shale deposits from the Maastrichtian Patti formation, Southern Bida basin, Nigeria. *Earth Sciences Research Journal*. 2012;**16**(2):139-150

[29] Burke K. The African plate. *South African Journal of Geology*. 1996;**99**:339-409

[30] Benkhelil J. The origin and evolution of the cretaceous Benue trough (Nigeria). *Journal of African Earth Sciences (and the Middle East)*. 1989;**8**(2-4):251-282

[31] Guiraud R, Bellion Y. Late carboniferous to recent, geodynamic evolution of the west Gondwanian, cratonic, Tethyan margins. *The Tethys Ocean*. 1995;**1**(1):101-124

[32] Reyment R. Ammonite biostratigraphy, continental drift and oscillatory transgressions. *Nature*. 1969;**224**(5215):137

[33] Murat RC. Stratigraphy and paleogeography of the cretaceous and lower tertiary in Southern Nigeria. In: Dessauvage TFJ, Whiteman AJ, editors. *African Geology*. Ibadan: Ibadan University Press; 1972. pp. 251-266

[34] Weber K, Daukoru E. Petroleum geological aspects of the Niger Delta. *Journal of Mining and Geology*. 1975;**12**(1/2):1-22

[35] Mebradu S. Palynofacies of Enugu/Iva valley shales Anambra State, Nigeria. *Journal of Mining and Geology*. 1990;**26**(1):13-20

[36] Ojo O. *Mineralogy and Chemical Mobility in some Weathered Ash Dump Sites*. South Africa: University of the Western Cape, South Africa; 2010

[37] Bortnikov N, Novikov V, Savko A, Boeva N, Zhegallo E, Bushueva E, et al. Structural-morphological features of kaolinite from clayey rocks subjected to different stages of lithogenesis: Evidence from the Voronezh anteklise. *Lithology and Mineral Resources*. 2013;**48**(5):384-397

[38] Nesbitt HW, Young GM. Early Proterozoic climates and plate motions inferred from major element chemistry of lutites. *Nature*. 1982;**299**:715-717

[39] Harnois L. The CIW index: A new chemical index of weathering. *Sedimentary Geology*. 1988;**55**: 319-322

[40] Fedo CM, Wayne Nesbitt H, Young GM. Unraveling the effects of potassium metasomatism in sedimentary rocks and paleosols, with implications for paleoweathering conditions and provenance. *Geology*. 1995;**23**(10):921-924

[41] Voicu G, Bardoux M, Harnois L, Crepeau R. Lithological and geochemical features of igneous and sedimentary rocks at the Omai gold mine, Guyana, South America. *Exploration and Mining Geology*. 1997;**2**(6):153-170

[42] Herron MM. Geochemical classification of terrigenous sands and shales from core or log data. *Journal of Sedimentary Research*. 1988;**58**(5):820-829

[43] Pettijohn FJ. *Sedimentary Rocks*. Vol. 2. New York: Harper & Brothers; 1957

[44] Gromet LP, Haskin LA, Korotev RL, Dymek RF. The "North American shale composite": Its compilation, major and trace element characteristics. *Geochimica et Cosmochimica Acta*. 1984;**48**(12):2469-2482

- [45] Turekian KK, Wedepohl KH. Distribution of the elements in some major units of the earth's crust. *Geological Society of America Bulletin*. 1961;72(2):175-192
- [46] Taylor SR, McLennan SM. The geochemical evolution of the continental crust. *Reviews of Geophysics*. 1995;33(2):241-265
- [47] Turekian KK, Wedepohl KH. Distribution of the elements in some major units of the Earth's crust. *Geological Society of America Bulletin*. 1961;72:175-192. DOI: 10.1130/0016-7606(1961)72[175:DOTAIS]2.0.CO;2
- [48] Taylor SR, McLennan SM. *The Continental Crust: Its Composition and Evolution: An Examination of the Geological Record Preserved in Sedimentary Rocks*. Oxford, UK: Blackwell; 1985. 328 pp
- [49] Nesbitt H, Young G, McLennan S, Keays R. Effects of chemical weathering and sorting on the petrogenesis of siliciclastic sediments, with implications for provenance studies. *The Journal of Geology*. 1996;104(5):525-542
- [50] Nesbitt H, Young GM. Formation and diagenesis of weathering profiles. *The Journal of Geology*. 1989;97(2):129-147
- [51] Duzgoren-Aydin N, Aydin A, Malpas J. Re-assessment of chemical weathering indices: Case study on pyroclastic rocks of Hong Kong. *Engineering Geology*. 2002;63(1-2):99-119
- [52] Bock B, McLennan S, Hanson G. Geochemistry and provenance of the middle Ordovician Austin Glen member (Normanskill formation) and the Taconian orogeny in New England. *Sedimentology*. 1998;45(4):635-655
- [53] Elzien S, Farah A, Alhaj A, Mohamed A, Al-Imam O, Hussein A, et al. Geochemistry of Merkhayat Sandstones, Omdurman Formation, Sudan: Implication of depositional environment, provenance and tectonic setting. *International Journal of Geology, Agriculture and Environmental Sciences*. 2014;2(3):10-15
- [54] McLennan SM, Taylor S, Eriksson K. Geochemistry of Archean shales from the Pilbara Supergroup, western Australia. *Geochimica et Cosmochimica Acta*. 1983;47(7):1211-1222
- [55] Mongelli G. Trace elements distribution and mineralogical composition in the < 2- $\mu$ m size fraction of shales from the Southern Apennines, Italy. *Mineralogy and Petrology*. 1995;53(1-3):103-114
- [56] Gu XX, Liu JM, Zheng MH, Tang JX, Qt L. Provenance and Tectonic setting of the Proterozoic turbidites in Hunan, South China: Geochemical evidence. *Journal of Sedimentary Research*. 2002;72:393-407
- [57] Nyakairu GW, Koeberl C. Mineralogical and chemical composition and distribution of rare earth elements in clay-rich sediments from Central Uganda. *Geochemical Journal*. 2001;35(1):13-28
- [58] Suttner LJ, Dutta PK. Alluvial sandstone composition and paleoclimate; I, framework mineralogy. *Journal of Sedimentary Research*. 1986;56(3):329-345
- [59] Dickinson WR. Interpreting provenance relations from detrital modes of sandstones. *Provenance of Arenites*. 1985;148:333-361
- [60] Dickinson WR. Provenance and sediment dispersal in relation to

- paleotectonics and paleogeography of sedimentary basins. In: Kleinspehn KL, Poala C, editors. *New Perspective in Basin Analysis*. New York: Springer; 1988. pp. 3-25
- [61] Etemad-Saeed N, Hosseini-Barzi M, Armstrong-Altrin JS. Petrography and geochemistry of clastic sedimentary rocks as evidences for provenance of the lower Cambrian Lalun formation, Posht-e-badam block, Central Iran. *Journal of African Earth Sciences*. 2011;**61**(2):142-159
- [62] Perri F. Composition, provenance and source weathering of Mesozoic sandstones from Western-Central Mediterranean alpine chains. *Journal of African Earth Sciences*. 2014;**91**:32-43
- [63] Saxena A, Pandit M. Geochemistry of Hindoli group metasediments, SE Aravalli craton, NW India: Implications for palaeoweathering and provenance. *Journal of the Geological Society of India*. 2012;**79**(3):267-278
- [64] Wang B-Q, Wang W, Zhou M-F. Provenance and tectonic setting of the Triassic Yidun group, the Yidun terrane, Tibet. *Geoscience Frontiers*. 2013;**4**(6):765-777
- [65] Xu Y, Du Y, Cawood PA, Yang J. Provenance record of a foreland basin: Detrital zircon U–Pb ages from Devonian strata in the North Qilian Orogenic Belt, China. *Tectonophysics*. 2010;**495**(3-4):337-347
- [66] Zaid SM, Elbadry O, Ramadan F, Mohamed M. Petrography and geochemistry of pharaonic sandstone monuments in Tall San Al Hagr, Al Sharqiya Governorate, Egypt: Implications for provenance and tectonic setting. *Turkish Journal of Earth Sciences*. 2015;**24**(4):344-364
- [67] Crook KAW. Lithogenesis and tectonics: The significance of compositional variation in flysch arenites (greywackes). In: Dott RH, Shaver RH, editors. *Modern and Ancient Geosynclinal Sedimentation*, Special Publication 19. Society of Economic Geologists and Paleontologists; 1974. pp. 304-310
- [68] Hayashi K-I, Fujisawa H, Holland HD, Ohmoto H. Geochemistry of ~ 1.9 Ga sedimentary rocks from northeastern Labrador, Canada. *Geochimica et Cosmochimica Acta*. 1997;**61**(19):4115-4137
- [69] Paikaray S, Banerjee S, Mukherji S. Geochemistry of shales from the Paleoproterozoic to Neoproterozoic Vindhyan Supergroup: Implications on provenance, tectonics and paleoweathering. *Journal of Asian Earth Sciences*. 2008;**32**(1):34-48
- [70] Floyd P, Winchester J, Park R. Geochemistry and tectonic setting of Lewisian clastic metasediments from the early Proterozoic Loch Maree Group of Gairloch, NW Scotland. *Precambrian Research*. 1989;**45**(1-3):203-214
- [71] Hiscott RN. Ophiolitic source rocks for Taconic-age flysch: Trace-element evidence. *Geological Society of America Bulletin*. 1984;**95**(11):1261-1267
- [72] Floyd PA, Leveridge BE. Tectonic environment of the Devonian Gramscatho basin, south Cornwall: Framework mode and geochemical evidence from turbiditic sandstones. *Journal of the Geological Society London*. 1987;**144**:531-542
- [73] Ortiz E, Roser BP. Major and trace element provenance signatures in stream sediments from the Kando river, San'in district, southwest Japan. *Island Arc*. 2006;**15**:223-238



[74] Cullers RL, Berendsen, P. The Provenance and chemical variation of sandstones associated with the mid-continent rift system, USA. *European Journal of Mineralogy*. 1998;**10**:987-1002. DOI: 10.1127/ejm/10/5 /0987

[75] Taylor SR. Geochemistry of Andesites. In: Ahrens LH, editor. *Origin and Distribution of the Elements*. Vol. 30. International Series of Monographs in Natural Philosophy; 2015, 2015. pp. 559-582

[76] Ogbahon O, Olujinmi O. Geochemistry of Maastrichtian clastic sedimentary rocks from Western flank of Anambra Basin, Nigeria: Implications for provenance, tectonic setting, paleoclimate and depositional paleoenvironment. *International Journal of Geosciences*. 2019;**10**:91-118. DOI: 10.4236/ijg.2019.101007

[77] Bhatia MR, Crook KA. Trace element characteristics of graywackes and tectonic setting discrimination of sedimentary basins. *Contributions to Mineralogy and Petrology*. 1986;**92**(2):181-193

[78] Maynard JB, Valloni R, Yu HS. Composition of modern deep-sea sands from arc-related basin. In: Leggett JK, editor. *Trench Forearc Geology: Sedimentation and Tectonics on Modern and Ancient Active Plate Margins*. Vol. 10. *Geol.Soc. Lond. Spec. Pub.*; 1982. pp. 551-561